



A 7500-year strontium isotope record from the northwestern Nile delta (Maryut lagoon, Egypt)



Clément Flaux ^{a,*}, Christelle Claude ^a, Nick Marriner ^{a,b}, Christophe Morhange ^a

^a Aix-Marseille University, CNRS-IRD-Collège de France, UM34 CEREGE, BP 80, 13545 Aix-en-Provence Cedex 4, France

^b Laboratoire Chrono-Environnement, UMR 6249 CNRS, Université de Franche-Comté, UFR ST, 25030 Besançon, France

ARTICLE INFO

Article history:

Received 3 December 2012

Received in revised form

19 June 2013

Accepted 22 June 2013

Available online

Keywords:

⁸⁷Sr/⁸⁶Sr

Ostracods

Nile

Delta

Mediterranean

Palaeohydrology

Holocene

African Humid Period

Alexandria

ABSTRACT

During the Holocene, delta evolution has been collectively mediated by relative sea-level changes, continental hydrology and human impacts. In this paper, we present a strontium isotope record from the Maryut lagoon (northwestern Nile delta) to quantify the interplay between relative sea-level variations and Nile flow changes during the past 7500 years. ⁸⁷Sr/⁸⁶Sr stratigraphy allows five hydrological stages to be defined. (1) The marine transgression of the area is dated to ~7.5 ka cal. BP, with a clear marine ⁸⁷Sr/⁸⁶Sr signature (0.70905–0.7091). (2) Between ~7 and ~5.5 ka, in the context of the so-called African Humid Period (AHP), freshwater inputs became progressively predominant in the Maryut's hydrology. Deceleration of sea-level rise coupled with high Nile discharge induced coastal progradation which led to the progressive closure of the Maryut lagoon. (3) Between ~5.5 and ~3.8 ka, the end of the AHP is translated by a progressive hydrological shift from a Nile-dominated to a marine-dominated lagoon (⁸⁷Sr/⁸⁶Sr shifts from 0.70865 to 0.7088 to 0.70905–0.70915). (4) From ~2.8 to ~1.7 ka, ⁸⁷Sr/⁸⁶Sr ratios shift towards lower values (0.7084). Although this change is not precisely resolved because of a hiatus in the Maryut's sedimentary record, the ⁸⁷Sr/⁸⁶Sr transition from sea-like to Nile-dominated values is attributed to irrigation practices since the early Ptolemaic period (i.e. since ~2.3 ka), including the Alexandria canal which played a key role in isolating the Maryut from the Mediterranean sea. (5) The final phase of the record covers the period between ~1.7 and ~0.2 ka. ⁸⁷Sr/⁸⁶Sr ratios indicate high freshwater inputs (from 0.7080 to 0.7085), except between 1.2 and 1.1 to ~0.7 ka, when a Maryut lowstand and seawater intrusion are attested. In modern times, the Nile's coastal lagoons have been increasingly supplied by freshwater linked to the diversion of waters from the two Nile branches into the irrigation system. It is suggested that this process began in early Antiquity and has engendered a reduction in the number of Nile branches from seven in ancient times to just two at present.

© 2013 Elsevier Ltd. All rights reserved.

1. Introduction

Today, hydrological changes in deltaic settings have important implications for coastal ecosystems, agriculture, fishery activities, freshwater resources and human geographies (Svytski et al., 2009). With reference to the Nile delta, during the 20th century, river-channel modifications, artificial waterways and a series of dams have diverted around one third of Nile water (Stanley, 1996). Increasing freshwater discharge from the delta's canal system has led to desalinization of the lagoons (Bernaconi and Stanley, 1994), with implications for the management of fisheries. Paradoxically,

rising relative sea level (Frihy et al., 2010), coastal erosion (Frihy and Lawrence, 2004), deltaic subsidence (Becker and Sultan, 2009) and the recycling of sewage water have engendered soil salinization in the northern delta (Kotb et al., 1999). Long-term changes in the coastal hydrology of the Nile delta therefore reflect the complex interplay, at decadal to centennial timescales, between climate forcing, human management and local geomorphological responses.

Past fluctuations in the Holocene water budget provide insights into the drivers and amplitude of hydrological changes on the Nile delta coast. Previous research has described the early Holocene marine transgression of the late Pleistocene alluvial plain (see Stanley and Warne, 1993a; Butzer, 2002). The present Nile coast, characterized by widespread lagoons and marshes behind a nearly continuous coastal sand barrier, began to form at ca 7.5 ka cal. BP,

* Corresponding author.

E-mail address: flaux@cerege.fr (C. Flaux).

under the cumulative action of a deceleration in sea-level rise and the rapid influx of sediments (Stanley and Warne, 1993a). Since this time, (1) relative sea-level variations (Stanley and Warne, 1993b; Stanley and Toscano, 2009; Marriner et al., 2012a), (2) changes in Nile discharge and sediment load (Foucault and Stanley, 1989; Said, 1993; Revel et al., 2010, 2013; Williams et al., 2010; Bernhardt et al., 2012; Marriner et al., 2012b; Blanchet et al., 2013) and (3) early irrigation and drainage practices on the delta (Butzer, 1976; Said, 1993; Shaw, 2000), have induced significant water budget changes. To date, however, the coastal water budget has not been quantified for the Holocene period. Previous work has focused upon palaeontological proxies, which only yield qualitative insights into the evolution of the water budget on the Nile coast (Bernaconi and Stanley, 1994; Flaux et al., 2011).

Faunal assemblages in lagoon sediments must be used in conjunction with others indicators to quantify palaeohydrological changes. Reinhardt et al. (1998, 2001) demonstrated that faunal assemblages and the Sr isotopic composition of coastal shells is a reliable proxy to quantify the modern water budget on the Nile coast. In this paper, we adopt the same approach for the Maryut lagoon and look to generate a time series for the mid to late Holocene sequence. This time series helps to quantify the interplay between relative sea-level variations and Nile palaeohydrology in modulating lagoonal water budgets during the last 7500 years.

We selected the Maryut lagoon because: (1) its location at the margin of the delta makes it sensitive to hydrological changes, particularly phases of deltaic extension and retraction; and (2) the lagoon has been a key feature of Alexandria's hinterland economy since Antiquity (Empereur, 1998; Blue and Khalil, 2010; Blue et al., 2011). Its shores accommodated major production centres and the lagoon acted as a gateway to the Nile and the rest of Egypt. Sr isotopic ratios measured in the Maryut's Holocene archives have allowed us to evaluate the climatic, geomorphological and anthropogenic processes that have controlled hydrological

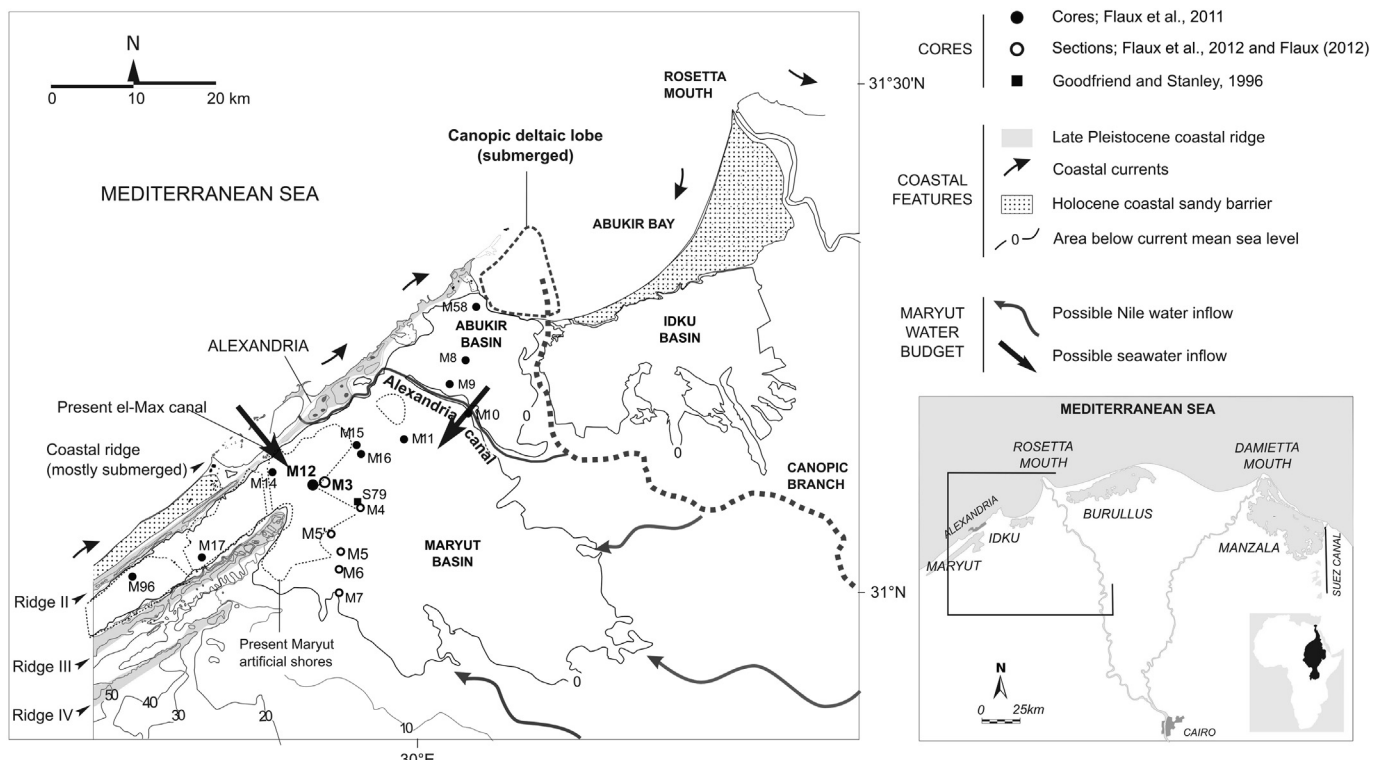
modifications in the northwestern Nile delta and the Alexandria region during the last 7500 years.

2. Study site and methods

2.1. Hydrological context

The Maryut lagoon is partially isolated from the sea, behind consolidated late Pleistocene coastal ridges (Fig. 1; El-Asmar and Wood, 2000). An outlet into the sea existed through Abu Qir lagoon (completely drained today, Fig. 1; Flaux et al., 2011) before the completion of the Alexandria canal at least 2000 years ago (Hairy and Sennoune, 2006). Another outlet may have existed through the present-day El Mexx canal (Fig. 1). Nile inflow to the Maryut was supplied by at least two tributaries, linked to the former Canopic branch (Fig. 1; Trampier, 2009; Flaux, 2012). The latter was the westernmost branch of the Nile and has progressively silted up during the past 2000 years (Fig. 1; Toussoun, 1922; Bernand, 1970; Chen et al., 1992; Stanley et al., 2004a; Hairy and Sennoune, 2006). Local precipitation is negligible, given the semi-arid to arid climatic context of the area (Butzer, 2002). The Sr isotopic composition of Maryut ostracods therefore essentially results from a mixing between Nile water and seawater (Fig. 1).

Sr behaves conservatively in estuarine and brackish environments (Ingram and Sloan, 1992; Reinhardt et al., 1998). In contrast to oxygen isotopes, strontium isotopes show no measurable fractionation with temperature or other physical environmental changes (Faure and Powell, 1972; Gosz et al., 1983; Hart et al., 2004; Lance et al., 2011). Biogenic carbonates incorporate Sr in their crystal lattices without any vital effects (Durazzi, 1977; Graustein, 1989; Reinhardt et al., 1999; Holmes et al., 2007) and therefore record the $^{87}\text{Sr}/^{86}\text{Sr}$ of the water in which they grew. The Sr composition of Nile water ($^{87}\text{Sr}/^{86}\text{Sr} = 0.706$; [Sr] = 0.235 ppm; Brass, 1976; Gerstenberger et al., 1999) is well differentiated from



seawater ($^{87}\text{Sr}/^{86}\text{Sr} = 0.709172$; [Sr] = 9 ppm; Hodell et al., 1990). This geochemical contrast allowed us to evidence variations in the Maryut lagoon water budget.

2.2. Sampling and analytical methods

Ostracods taken from section M3 and cores M12 and M12bis (Fig. 1) were selected for strontium analyses. Cores M12 and M12bis are 9 m long and constitute the longest sequences in the Maryut area. Section M3, located close to M12, was selected because at this site the upper part of the Maryut stratigraphy has not been reworked by recent human activities. This section of the Maryut's upper stratigraphy allows a better identification of bio-sedimentological units and a finer sampling resolution.

Microfauna was separated from the terrigenous fraction using a 200 μm sieve. We selected the euryhaline ostracod *Cyprideis torosa*, present throughout most of the sequence, because the species has a wide tolerance to salinity, from lightly brackish to hypersaline environments (Athersuch et al., 1989; Frenzel and Boomer, 2005). At least 30 valves were extracted from each sample. Clean shells were selected and washed with milliQ water and then dissolved in a 3 N HNO₃ solution. In gypsum-rich samples, ~30 clean and translucent gypsum crystals were sampled from the sandy fraction. Gypsum was then dissolved in 3 N HNO₃. For both carbonate shells and gypsum samples, we centrifuged before selecting the supernatant so as to avoid Sr contamination by possible undissolved residues. Sr purification techniques are reported in Ollivier (2006). Sr isotopic measurements were performed on a Finnegan MAT 262 multicollector thermo ionization mass spectrometer (TIMS). Possible isobaric interferences from ^{87}Rb were carefully checked using ^{85}Rb . Total procedure blanks were below 10 ng, which is negligible compared to the 1 μg Sr sample sizes used. Fifteen replicate analyses of the NBS 987 standard yielded an $^{87}\text{Sr}/^{86}\text{Sr}$ of 0.710265 ± 0.000046 (2σ). All Sr ratios have been normalized to an NBS 987 $^{87}\text{Sr}/^{86}\text{Sr}$ certified value of 0.710248 (Table 2). The freshwater detection limit is $^{87}\text{Sr}/^{86}\text{Sr} = 0.709126$, with a reported error in the Sr isotopic ratio of 46 ppm, subtracted from the seawater signature (see Fig. 3). Measured $^{87}\text{Sr}/^{86}\text{Sr}$ constitutes an apparent value; it is the mean equivalent of the time-range represented by the bulk sample thickness. Most of the sample ages range between ~150 and ~250 years (see Fig. 3). Therefore, seasonal to multi-decadal changes in Nile flow cannot be resolved by our data. Instead, we have focused upon centennial to millennial-scale hydrological changes during the Holocene.

In addition, the relative mass of biogenic material and *C. torosa* abundance in bulk samples were used as proxies for the lagoon's biomass production through time, because shells were deposited *in situ* and were well preserved in the sediment (Flaux et al., 2011). These time-series have been compared and contrasted with the Sr data.

2.3. Chronological framework

The age model is based on 32 radiocarbon dates, compiled from cores taken in the northwestern Nile delta area (for core location and references see Fig. 1). Carbonate samples comprise mainly connected lagoon shells (*Cerastoderma glaucum*). Organic samples constitute wood and organic-rich lenses taken within the sediment sequence. Most of the samples were taken at stratigraphic boundaries within the Holocene sequence. The dataset is represented in the form of a summed Probability Density Function plot (PDF; Fig. 2A). Narrower PDF peaks can be noted at the late Pleistocene boundary, and between units 1–2, 2–3 and 3–4 (Fig. 2A). For these four well-dated stratigraphic boundaries of the Maryut's lower sequence, the mean age $\pm 2\sigma$ was used for calibration

(Table 3). Reservoir ages used for calibration are discussed in Section 4.1. Sedimentation rates in cores M12 and M12bis and section M3 were then calculated, based on the stratigraphic boundary's calibrated age. For the upper sequence, the complexity of the stratigraphy, as well as lateral changes and reworking at the top of the cores did not allow us to employ the same methodology. We used the age model defined in Flaux et al. (2012).

3. Results

The Maryut's Holocene sequence lies above late Pleistocene stiff muds that were deposited in an inland sebkha in proximity to a former branch of the Nile (Chen and Stanley, 1993). Table 1 summarizes previous bio-sedimentary results including grain size analyses, faunal assemblages and gypsum identification (Flaux et al., 2011, 2012). We have identified six units above the late Pleistocene surface. The first unit comprises dark grey silty clay. The matrix includes abundant lagoonal shells and shell debris. The relative proportion of biogenic and biodetrinitic fractions is ~25 %. This facies was interpreted as being a marine-influenced lagoon that indicates a perennial connection between the lagoon and the sea. The second unit is mostly composed of dark grey silty clay, which is compact and homogeneous. The biogenic fraction drops to 0–4% of the aggregate sediment mass. Only a few specimens of *C. torosa* were found within the matrix, indicating a confined lagoon, i.e. a distal lagoon with a low rate of seawater replenishment (Guelorget and Perthuisot, 1983). The third unit is very similar to the first one, comprising dark muds rich in lagoonal shells, which constitute up to 30% of the sediment aggregate. Clear alternations between shell and mud layers were observed at a centimetric scale. These cycles suggest that the lagoon bottom was colonized by benthic species before being rapidly buried by muds during Nile floods. Compared to the second unit, the faunal assemblages indicate a return to marine-dominated conditions. The fourth unit was characterized by light brown clayey silt. The appearance of lightly brackish species attests to a brackish to lightly-brackish lagoon with higher Nile inflow (Table 1), although the mixing with lagoonal species *sensu stricto* (Table 1) translates water budget fluctuations between Nile and marine inputs (Bernasconi and Stanley, 1994). The two faunal groups were found together within the same aggregate sample, probably because of rapid hydrological changes (e.g. in the modern Manzala lagoon, Reinhardt et al., 1998, 2001). In the fifth unit, mud deposits were accompanied by *in situ* gypsum crystals which represent between 20 and 50% of the sediment aggregate. With the exception of a few specimens of *C. torosa*, benthic fauna did not live within this evaporitic environment. The facies was interpreted as a periodically flooded sebkha (Flaux et al., 2012). Finally, faunal assemblages and sedimentary features of the sixth unit attest to similar hydrological conditions to unit 4, i.e. fluctuations between Nile and marine-dominated inputs (Table 1).

In summary, the Maryut's Holocene sequence comprises high proportions of silts and clays indicating that the Maryut has always been a low-energy decantation basin in a distal location to the closest Nile (Canopic) branch (Fig. 1). Sands and gravels deposited within these muds were mainly *in situ* biological fossils. The relative biogenic fraction of the sequence varied between 0 and 40% (Fig. 3B). The abundance of *C. torosa* varied between <10 and ~10,000 valves per 10 g of sediment aggregate (Fig. 3C). The two proxies showed a similar trend up the sequence, with higher values in the marine-influenced lagoon and the lightly brackish biofacies, and lower values in the confined lagoon and sebkha biofacies.

Sedimentation rates were calculated for all radiocarbon couples from cores taken on the northwestern Nile delta. A total of 75 radiocarbon dates were used for these calculations (see Flaux, 2012

Table 1

Sedimentary features and faunal composition of biofacies from the Maryut lagoon sequence. Data from cores M3, M12 and M12bis (location Fig. 1). Original data in Chen and Stanley (1993) (the late Pleistocene unit), Flaux et al., 2011 (units 1, 2, 3), Goodfriend and Stanley, 1996 (unit 4) and Flaux et al., 2012 (units 4, 5, 6).

Age/unit	Thickness range (m)	Color/texture/structure	Biogenic relative mass	Ecological bio-indicators and relative abundance (A: abundant/dominant species; B: rare/accessory species)		Gypsum form	Ecological and geomorphological meaning	
				Low-brackish	Lagoon <i>sensu stricto</i>			
Late Pleistocene	0.3–3	Greenish – grayish clayey silt. Numerous Oxidized patches and carbonates nodules	~0%	–	B: <i>Cyprideis torosa</i> (ostracod)	–	Inland playa, in proximity of Nile channel	
Holocene	1	0–0.2	Shelly dark muds	~25%	–	A: <i>Cyprideis torosa</i> (ostracod) <i>Ammonia beccarii</i> (foraminifera) <i>Cerastoderma glaucum</i> (bivalve) <i>Hydrobia</i> sp. (gastropod)	–	Marine influenced euryhaline lagoon
	2	0–4.2	Dark muds	0–4%	–	B: <i>Cyprideis torosa</i> (ostracod) <i>Ammonia beccarii</i> (foraminifera) <i>Hydrobia</i> sp. (gastropod)	Syn- and postsedimentary gypsum crystals	Confined lagoon (disconnected to the sea at least periodically)
	3	1.3–2.6	Shelly dark muds Centimetric alternation deposit of dark muds and shells layers	15–40%	–	A: <i>Cyprideis torosa</i> (ostracod) <i>Ammonia beccarii</i> (foraminifera) <i>Cerastoderma glaucum</i> (bivalve) <i>Hydrobia</i> sp. (gastropod) B: <i>Scrobicularia plana</i> (bivalve) <i>Loripes</i> sp. (bivalve) <i>Pirenella conica</i> (gastropod)	–	Marine influenced euryhaline lagoon
	4	0.15–0.2	Brown to grayish muds	5–15%	B: <i>Menaloides tuberculata</i> (gastropod) <i>Chara tomentosa</i> (Characea) <i>Chara zeylanica</i> (Characea)	A: <i>Cyprideis torosa</i> (ostracod) B: <i>Ammonia beccarii</i> (foraminifera) <i>Cerastoderma glaucum</i> (bivalve) <i>Hydrobia</i> sp. (gastropod)	Mycelium-like postsedimentary gypsum	Brackish to lowbrackish lagoon
	5	0–1.1	Grey to dark grey sandy muds. Some gypsum deposit in alternation with dark grey muds deposit. Muds cracks.	~0%	–	B: <i>Cyprideis torosa</i> (ostracod) <i>Hydrobia</i> sp. (gastropod)	20–50% of the bulk. Synsedimentary gypsum.	Sebkha periodically flooded
	6	0–0.65	Grey to dark grey muds. Organic layers.	5–15%	B: <i>Menaloides tuberculata</i> (gastropod) <i>Corbicula fluminalis</i> (bivalve) <i>Gyraulus</i> sp. (gastropod) <i>Limnaea</i> sp. (gastropod)	A: <i>Cyprideis torosa</i> (ostracod) <i>Ammonia beccarii</i> (foraminifera) <i>Hydrobia</i> sp. (gastropod) B: <i>Scrobicularia plana</i> (bivalve) <i>Loripes</i> sp. (bivalve) <i>Pirenella conica</i> (gastropod)	Mycelium-like postsedimentary gypsum.	Brackish to low-brackish lagoon

Table 2

Sr isotope data from the ostracod *Cyprideis torosa* and from gypsum extracted in cores M12 and M12bis and section M3. Fifteen replicate analyses of the NBS 987 standard yielded a $^{87}\text{Sr}/^{86}\text{Sr}$ ratio of 0.710265 ± 0.000046 (2σ). All Sr ratios measured in this work have been normalized to an NBS 987 $^{87}\text{Sr}/^{86}\text{Sr}$ certified value of 0.710248.

Core	Depth b msl (cm.)	Units	Material	Ostracod valves number	$^{87}\text{Sr}/^{86}\text{Sr}$
M12	395–420	5	Gypsum	—	0.709071
M12	400–425	5	Shells	31	0.708802
M12	440–450	5	Gypsum	—	0.708992
M12	485–495	5	Gypsum	—	0.708839
M12	495–505	4	Shells	35	0.708557
M12	505–525	4	Shells	29	0.708576
M12	540–575	3	Shells	35	0.708603
M12	590–625	3	Shells	32	0.709085
M12	640–675	3	Shells	40	0.709117
M12	675–700	3	Shells	35	0.709087
M12	725–750	3	Shells	30	0.709000
M12	750–775	3	Shells	35	0.709012
M12	775–785	3	Shells	40	0.709153
M12	1175–1195	2	Shells	38	0.709074
M12	825–850	2	Shells	30	0.708915
M12	850–875	2	Shells	27	0.708731
M12	890–925	2	Shells	30	0.708800
M12	990–1025	2	Shells	30	0.708700
M12	1040–1075	2	Shells	38	0.708804
M12	1140–1175	2	Shells	38	0.709055
M12	1195–1215	1	Shells	40	0.709094
M12	1215–1225	1	Shells	39	0.709122
M12bis	620–655	3	Shells	75	0.709140
M12bis	655–690	3	Shells	65	0.709120
M12bis	690–725	3	Shells	44	0.709120
M12bis	725–760	3	Shells	66	0.709018
M12bis	1180–1190	1	Shells	70	0.709103
M12bis	1190–1195	1	Shells	49	0.709114
M12bis	1145–1180	1	Shells	27	0.709084
M12bis	1195–1215	1	Shells	43	0.709139
M12bis	1215–1250	Late pleistocene	Shells	11	0.708855
M3	365–380	6	Shells	60	0.708685
M3	380–394	6	Shells	29	0.708429
M3	394–398	6	Shells	29	0.708664
M3	394–398	5	Gypsum	—	0.708897
M3	398–402	5	Gypsum	—	0.709034
M3	403–408	5	Gypsum	—	0.708991
M3	410–430	5	Gypsum	—	0.708929
M3	438–442	4	Shells	50	0.708086
M3	444–448	4	Shells	60	0.708396
M3	448–452	4	Shells	60	0.708393
M3	463–468	3	Shells	30	0.708783
M3	468–470	3	Shells	27	0.709083

for further details). Each couplet indicates a mean sedimentation rate for a given point (one core) and period. The whole dataset is plotted in Fig. 3D and translates the spatially averaged sedimentation rate for the northwestern delta. The data clearly denotes a gradual decrease in sediment loadings from ~ 4 to 0 – 1.5 mm yr $^{-1}$ over the last 7500 years.

$^{87}\text{Sr}/^{86}\text{Sr}$ varied between 0.7081 and 0.7092 (Fig. 3D and Table 2). Higher values were recorded within marine-influenced lagoon facies (units 1 and 3), presenting a range of 0.7090–0.7092. In the confined biofacies (unit 2), Sr isotopic ratios decrease progressively down to 0.7087 in the middle of the unit before gradually increasing in unit 3. Ostracods taken in late Pleistocene sediments (cores M12 and M12bis), and at the top of unit 3 (core M12 and section M3), were characterized by $^{87}\text{Sr}/^{86}\text{Sr}$ values similar to those of the overlying biofacies, rather than the biofacies in which they were found (Fig. 3D). We attribute these points to mixing and reworking processes at the stratigraphic boundaries. For this reason, these points were subsequently removed from the

Sr isotope time series. The upper part of the sequence (units 4, 5 and 6) showed the lowest values for the whole sequence. However, the lightly-brackish biofacies displays a relatively wide range of $^{87}\text{Sr}/^{86}\text{Sr}$ values, namely 0.7081–0.7086 for unit 4 and 0.7084–0.7087 for unit 6 (Fig. 3D). Between the two, $^{87}\text{Sr}/^{86}\text{Sr}$ in gypsum crystals from the sebkha-like biofacies (unit 5) showed higher radiogenic values, ranging between 0.7088 and 0.7091 (Fig. 3D).

4. Discussion

4.1. Marine reservoir age and hard water effects

Radiocarbon ages obtained from carbonate-rich samples in coastal areas need to be corrected for marine reservoir effects (i.e. the difference between the atmospheric radiocarbon content and the local ^{14}C content of the ocean surface water) and hard water effects resulting from the mixing of seawater and C-rich continental water. Recent studies in three western Mediterranean lagoons have demonstrated a reservoir age ranging between ~ 600 and ~ 1200 years (Zoppi et al., 2001; Sabatier et al., 2010). The hard water effect refers to the dilution of ^{14}C in the water body by the influx of continentally derived ^{14}C -free inorganic carbon. It can be estimated using the apparent ^{14}C age of lagoonal shells or organic matter taken in the topmost part of the sequence. A radiocarbon age obtained for a shell of *Cerastoderma* taken towards the top of the Maryut sedimentary sequence (section M3) indicated an apparent age of 345 ± 30 yr, while a thin organic layer ~ 10 cm below the latter sample yielded a similar age of 300 ± 30 yr (Flaux et al., 2012). These recent ages are coherent with the last stage of the Maryut sedimentary sequence, before it dried up in the late 18th century AD before being reclaimed in the late 19th century AD (Flaux et al., 2012). In light of this, samples were not corrected for a hard water effect. However, ^{14}C samples that were taken in a marine-dominated environment, as determined by the Sr isotopic ratio (see below), were corrected for a marine reservoir effect of 400 years, as established by Goiran (2001) in the bay of Alexandria.

4.2. Origin of strontium in the Maryut's palaeo-waters

Changes in $^{87}\text{Sr}/^{86}\text{Sr}$ measured in the fossil material of Maryut lagoon are related to changes in water balance between freshwater (Nile) and seawater (Mediterranean). However, changes in the composition of Nile water or seawater with time may alter the Maryut's Sr isotopic composition even though there have been no alterations in the water balance. The water budget could furthermore be mediated by changes in the regional precipitation and evaporation (E/P) regime during the Holocene (e.g. Zhao et al., 2012).

Because the residence time of Sr in the oceans is long (2.5 Ma; Hodell et al., 1990), compared to its short mixing time (around 1000 years, Capo et al., 1998), the $^{87}\text{Sr}/^{86}\text{Sr}$ value of the ocean reservoir is considered to be homogeneous and to have remained unchanged at the Holocene timescale (Capo and DePaolo, 1990; Hodell et al., 1990).

However, the strontium concentration and isotopic composition of Nile waters are needed to interpret changes in the Sr signature of Maryut waters. The Sr budget of the Nile derives from the fluvial weathering of the rocks and sediments that the water flows over or through. The main Nile comprises flow from three major tributaries that drain two catchments that differ in terms of age, geology and climatic regime (Woodward et al., 2007). The White Nile (WN) catchment is made-up of Pre-Cambrian crystalline basement in central Africa (Williams, 2009), while the Blue Nile (BN) and the Atbara River catchment is composed of Cenozoic volcanic basement, under monsoon-driven precipitation (Conway, 2000). At

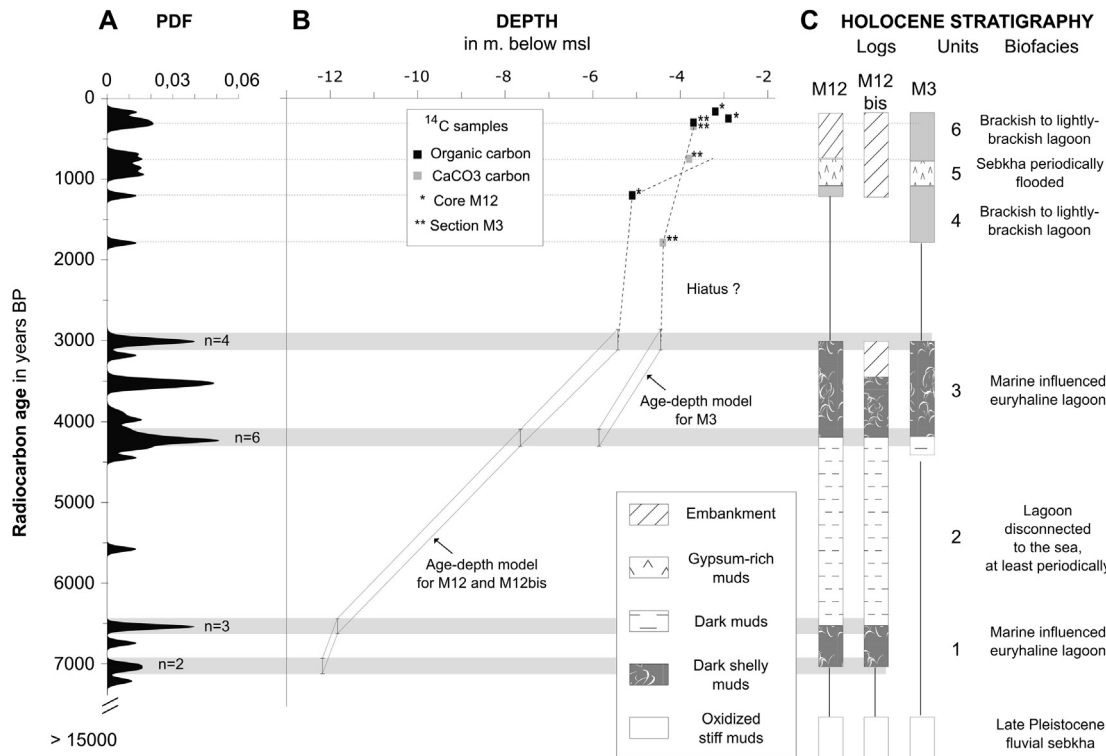


Fig. 2. A-Summed Probability Density Function (PDF) plot of thirty two radiocarbon dates compiled from cores taken in the northwestern Nile delta area (core locations are given in Fig. 1; original data from Goodfriend and Stanley, 1996; Flaux et al., 2011, 2012; Flaux, 2012). B-Age model for cores M12, M12bis and M3. Note the sedimentary hiatus between units 4 and 5, observed in both M12 and M3. C-Holocene biofacies and stratigraphic units in cores M12, M12bis and section M3, after Flaux et al. (2011, 2012). Hatching indicates reworked sediments, linked to modern human activities.

present, their hydrology and sediment loads are markedly different. The WN contributes almost a third of the total water discharge but only a minor proportion of the sediment load (3%), while the BN and Atbara River respectively account for 56% and 14% of the water discharge, and 72% and 25% of the sediment load (Foucault and Stanley, 1989). As a result, the present ⁸⁷Sr/⁸⁶Sr of Nile water and sediment measured in the main Nile is very similar to the BN signature (Krom et al., 1999; Revel et al., 2010). A change in precipitation pattern and erosion conditions in Nile catchments during the Holocene (i.e. a change in the relative fraction of WN, BN and

Atbara waters forming the main Nile) would have modified the Sr composition of Nile water entering the delta.

To date, no data on the main Nile's Sr isotope ratios are available for the Holocene period. However, ⁸⁷Sr/⁸⁶Sr of water and fine sediments (suspended fraction < 63 µm) of the modern main Nile (0.706 vs. 0.7047–0.7066; Brass, 1976; Gerstenberger et al., 1999; Krom et al., 1999; Revel et al., 2010; Padoan et al., 2011), the modern BN (0.7059 vs. 0.7054–0.7059; Palmer and Edmond, 1989; Krom et al., 2002; Box et al., 2011; Padoan et al., 2011) and the modern WN (0.7095–0.7109 vs. 0.7105–0.7111; Talbot et al., 2000;

Table 3

Radiocarbon data used in this study to refine the boundary ages. Sources: (1) Goodfriend and Stanley (1996); (2) Flaux et al. (2011, 2012). All shells used were formed within marine-dominated conditions, as demonstrated by the Sr isotopic ratio. ¹⁴C ages were corrected for the average reservoir age of seawater (400 yr), which is in agreement with the age of 370 ± 40 yr obtained for a pre-bomb shell of *Muricopsis trunculus* collected alive in Alexandria (Goiran, 2001). The Marine09 calibration curve (Reimer et al., 2009) and the software Calib 6.0 (Stuiver et al., 2005) were used for calibration.

Units boundary	Sources	Cod lab	Material	Section/core	¹⁴ C age ± analytical error	¹⁴ C age ± std. dev. (2σ)	Age range cal. BP
3–4	1	CAMS-18024	<i>Cerastoderma</i> sp.	S79	3010 ± 60	3010 ± 42	2710–2865
	2	SacA 11625	<i>Cerastoderma</i> gl.	M4	3030 ± 30		
	2	SacA 11628	<i>Cerastoderma</i> gl.	M3	3015 ± 30		
	2	SacA 11654	<i>Cerastoderma</i> gl.	M17	2985 ± 30		
2–3	1	AA-12434	<i>Cerastoderma</i> sp.	S79	4280 ± 50	4228 ± 83	4080–4545
	2	SacA 11622	<i>Cerastoderma</i> gl.	M4	4255 ± 30		
	2	SacA 11634	<i>Cerastoderma</i> gl.	M9	4220 ± 30		
	2	SacA 11643	<i>Cerastoderma</i> gl.	M10	4240 ± 30		
1–2	2	SacA 11639	<i>Cerastoderma</i> gl.	M12	4160 ± 30	6570 ± 95	6850–7290
	2	SacA 11655	<i>Cerastoderma</i> gl.	M17	4210 ± 30		
	2	SacA 11632	<i>Cerastoderma</i> gl.	M9	6540 ± 30		
	2	SacA 11633	<i>Cerastoderma</i> gl.	M9	6545 ± 30		
Late Pleistocene – Holocene	2	SacA 11642	<i>Cerastoderma</i> gl.	M12	6625 ± 30	7040 ± 85	7385–7680
	2	SacA 11644	Organic residues	M10	7010 ± 30		
	2	SacA 11645	<i>Cerastoderma</i> gl.	M10	7070 ± 30		

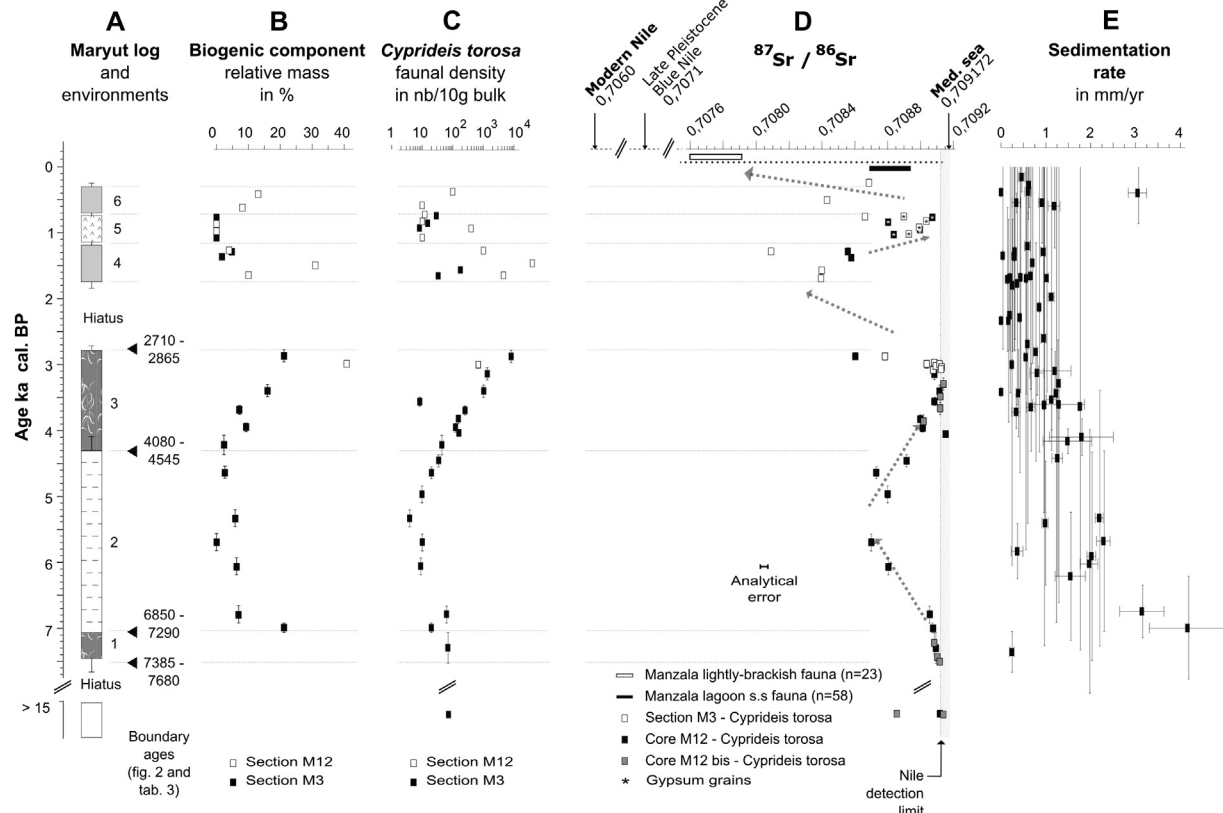


Fig. 3. A-Maryut summary log and palaeo-environments (legend in Fig. 2C), B—the relative mass of the biogenic fraction, C—relative abundance *C. torosa*, D— $^{87}\text{Sr}/^{86}\text{Sr}$ in *C. torosa* shells from the Maryut sequence plotted against time (calendar ages BP). For each sample, the vertical bar represents the age range of the aggregate sample in which the shells (~30) were sub-sampled. When not depicted, the vertical error bar is smaller than the symbol. Data for the modern Manzala lagoon are from Reinhardt et al. (1998, 2001). The Nile detection limit is the point at which the deviation of the $^{87}\text{Sr}/^{86}\text{Sr}$ measurement from the seawater value can be detected, taking into consideration the analytical error of 46 ppm. E—sedimentation rate in the northwestern Nile delta (Flaux et al., 2012).

Krom et al., 2002; Padoan et al., 2011) show that the $^{87}\text{Sr}/^{86}\text{Sr}$ of the dissolved fraction is similar to the higher radiogenic end of the isotope range of the suspended fraction. Moreover, late Pleistocene (~11.8 ka BP) $^{87}\text{Sr}/^{86}\text{Sr}$ of BN waters measured in molluscs displayed a ratio of 0.7071 (Talbot et al., 2000), while well-defined flood deposits, dated to 8.5–9 ka cal. BP, sampled in a prodelta core have been interpreted as “pure” BN sediment with a $^{87}\text{Sr}/^{86}\text{Sr}$ of 0.70685 (Revel et al., 2010, 2013). Therefore, the Sr isotopic ratios of the dissolved fraction of Nile waters should be reflected by $^{87}\text{Sr}/^{86}\text{Sr}$ in the suspended fraction. Because the latter proxy was measured by Krom et al. (1999, 2002) in Holocene sediments deposited in the Manzala lagoon (eastern delta), $^{87}\text{Sr}/^{86}\text{Sr}$ ratio measured in the fossil biogenic material of the Maryut lagoon can be used to reconstruct changes in mixing between seawater and Nile water.

Changes in Holocene precipitation and sea-spray inputs could potentially alter the Maryut's water budget. However, this component of the Sr isotopic budget is not considered in this study because the concentration of Sr in rainfall is generally several orders of magnitude lower (e.g. 4–40 ppb in eighteen rain samples from Israel, Herut et al., 1993) than that of the Nile (0.235 ppm) and seawater (8 ppm).

4.3. Palaeo-hydrology of the Maryut lagoon

Micropalaeontological and Sr isotope data elucidate the hydrological history of the Maryut since 7.5 ka cal. BP (Fig. 4). Changes in the water budget have been compared and contrasted with: (1) modelled relative sea level for the Carmel coast of Israel (Sivan

et al., 2001, 2004); (2) changes in Nile runoff reconstructed using Ti/Ca ratios (Blanchet et al., 2013); (3) relative precipitation in the Blue Nile watershed, derived from $\delta^{18}\text{O}$ of carbonates in lake Ashenge (Marshall et al., 2009); and (4) relative precipitation in the White Nile watershed derived from diatom data from Lake Victoria (Stager et al., 2003). At the local scale, possible human modification of the Maryut's hydrology, such as irrigation networks attested by historical sources (Flaux et al., 2012) are also depicted in Fig. 4.

4.3.1. Marine ingressions at ~7.5 ka

Lagoon sedimentation in the Maryut area began at ~7.5 ka. $^{87}\text{Sr}/^{86}\text{Sr}$ presents a clear seawater signature (Fig. 3D) that translates the Holocene marine transgression of the Maryut area. The base of the Holocene sequence in core M12 was measured at 12 m below msl and marks the relative sea level minimum at ~7.5 ka. It is consistent with regional models of sea-level rise (Sivan et al., 2001, 2004) suggesting that the sea level was ~10 m below msl at this time (Fig. 4). Sedimentation rates in the northwestern delta have progressively decreased during the last ~7500 years (Fig. 3E). We suggest that this was controlled by the gradual decline in sea-level rise during the same period. This interpretation is supported by the concept of accommodation space, which controls the basin's water depth and the potential for further sediment build-up (Einsele, 2000). It implies that the Maryut basin has not been significantly affected by vertical land movements (and subsequent relative sea-level rise) since the mid-Holocene, which contrasts with archaeological data from Aboukir Bay (Stanley et al., 2004b). Previous investigations of the Maryut's Holocene sequence (Warne and Stanley, 1993; Stanley and Warne,

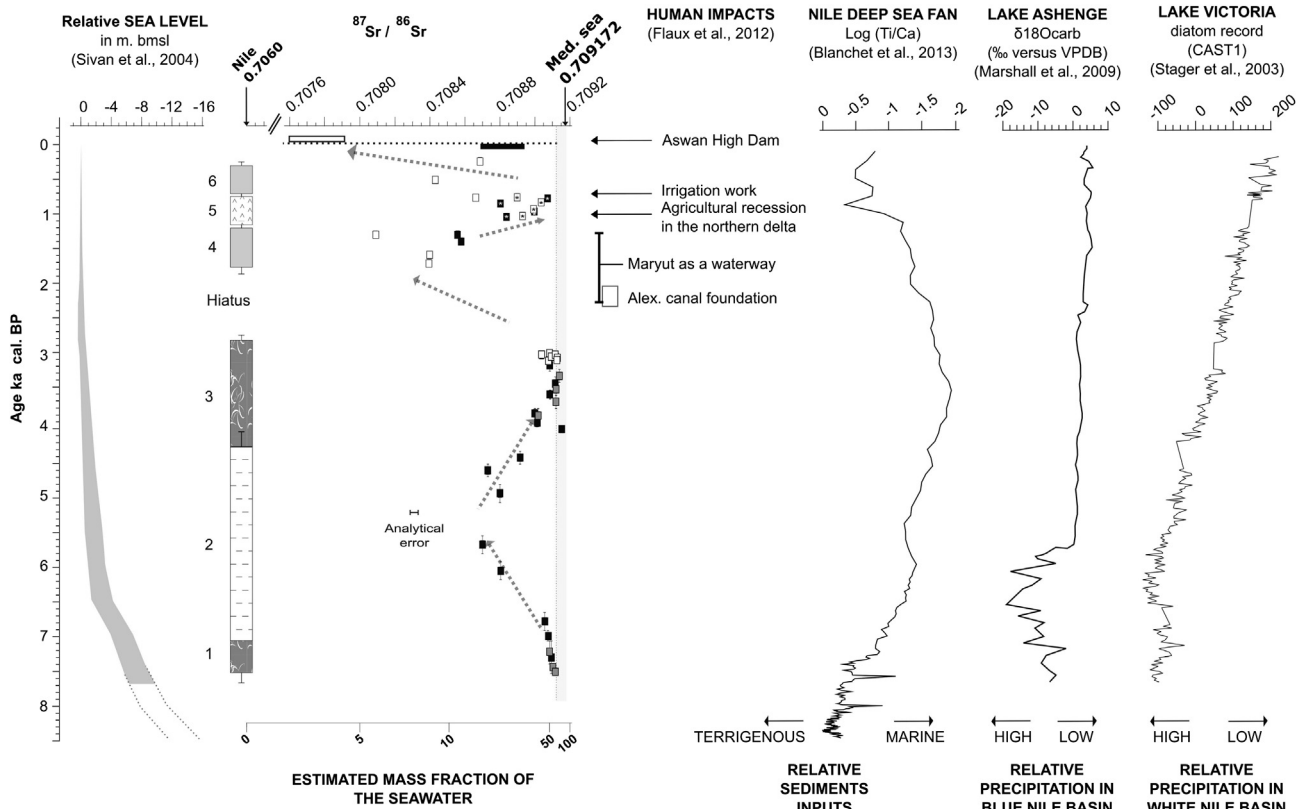


Fig. 4. $^{87}\text{Sr}/^{86}\text{Sr}$ in the Maryut sequence (see legend in Fig. 3) depicted alongside: relative sea-level modelled for the Carmel coast of Israel (Sivan et al., 2001, 2004), relative terrigenous and marine inputs in the Nile deep-sea fan (Blanchet et al., 2013), $\delta^{18}\text{O}$ of carbonates from lake Ashenge (Marshall et al., 2009), and diatom data from Lake Victoria (Stager et al., 2003; CAS1 mainly represents relative abundances of shallow and deep-water taxa and is therefore an estimate for lake depth). The mass fraction of seawater was estimated via a two-component mixing equation using modern seawater ($^{87}\text{Sr}/^{86}\text{Sr} = 0.709172$; $[\text{Sr}]_{\text{sw}} = 9 \text{ ppm}$; Hodell et al., 1990) and Nile river water ($^{87}\text{Sr}/^{86}\text{Sr} = 0.7060$; $[\text{Sr}] = 0.235 \text{ ppm}$; Brass, 1976; Gerstenberger et al., 1999) as the two end-members (e.g. Andersson et al., 1992).

1993a) yielded similar conclusions with regards to the relative vertical stability of the Maryut basin, although Marriner et al. (2012a) have recently elucidated probable compaction processes.

4.3.2. Deceleration of sea-level rise and progradation of the Nile delta coast between ~6.8 and ~5.5 ka cal. BP

Following the marine transgression of the Maryut depression, the Sr isotope ratio slowly shifted from marine values towards lower radiogenic values between ~6.8 and ~5.5 ka cal. BP (Fig. 3D). Sr isotope ratios reached a low of 0.7087 during this period consistent with higher Nile inflow into the lagoon that significantly diluted the former marine-dominated water budget. We suggest that this phase translates both: (1) the strong deceleration of sea-level rise (Morhange et al., 2001; Sivan et al., 2001, 2004); and (2) high Nile inflow recorded during the late African Humid Period (AHP), richly documented to have spanned ~12 up to ~5.5 ka cal. BP, recorded in eastern African lake levels (Gasse, 2000; Chalié and Gasse, 2002; Marshall et al., 2009, Fig. 4), sapropel deposition in the eastern Mediterranean (e.g. Weldeab et al., 2002; Box et al., 2011) and Nile floodplain geomorphology (Said, 1993; Woodward et al., 2007; Williams et al., 2010). On the Nile delta, it has been shown that the Sebennitic mouth prograded at least 15 km seaward between 8 and 6 ka (Stanley and Warne, 1993a; uncalibrated ^{14}C dates). In a broader context, major worldwide deltaic sequences were initiated between 8.5 and 6.5 ka BP because of the relative stabilisation of sea level around this time (Stanley and Warne, 1994; Hori et al., 2004). We suggest that the progradation of the Nile delta, and especially the Canopic lobe in the western delta (Fig. 1; Stanley et al., 2004a), led to the partial

isolation of the Maryut lagoon from the sea. Biogenic production during this phase reached low values (Fig. 3B and C), accompanied in the sand fraction by gypsum crystals, consistent with the confinement of the lagoon (Guelorget and Perthuisot, 1983), with reduced seawater exchanges (Flaux et al., 2011).

4.3.3. The mid- to late-Holocene pluvial/arid transition: ~5.5 to ~3.8 ka cal. BP

After ~5.5 ka cal. BP, $^{87}\text{Sr}/^{86}\text{Sr}$ ratios shift towards higher radiogenic values. A fully marine-like signature is recorded from ~3.8 to ~2.8 ka cal. BP. $^{87}\text{Sr}/^{86}\text{Sr}$ measured in fine sediments (<20 μm) from the Manzala's Holocene sequence, decreased from ~0.7087 to ~0.7077 between ~6 and ~5 ka cal. BP (core S21; Krom et al., 2002). As previously discussed, Sr in the suspended load is very similar to the dissolved fraction (see Section 4.2). Therefore, it is suggested that the main Nile waters' Sr isotopic ratio decreased in a similar manner to the suspended load measured in core S21. In the Maryut lagoon, however, the Sr ratios' shift towards higher radiogenic values between ~5.5 and ~3.8 ka cal. BP, consistent with an inflow of seawater into the lagoon. Accordingly, the diversity and abundance of the lagoon's biota describes a similar trend during this period. This ecological response also translates the enhancement of water exchange between the lagoon and the sea, as demonstrated in a study of numerous present-day marginal marine environments (Guelorget and Perthuisot, 1983).

Several causes can explain the increase in seawater in the lagoon's water budget between ~5.5 and ~3.8 ka cal. BP. Storm surges are short timescale events that introduce seawater into lagoons. However, there was no evidence of storm impacts in the

studied cores or, for that matter, in other cores from the Maryut lagoon (Flaux, 2012). Moreover, the progressive increase in marine influence evokes longer, millennial-scale processes. Relative sea-level rise was minor in the study area because the rate of eustatic sea-level rise slowed during this period (Fleming et al., 1998; Sivan et al., 2001, 2004; Fig. 4) and significant land-level drops can be ruled out. A final cause is the reduction of Nile inflow to the lagoon, considering that the Maryut's inflow is primarily a balance between Nile waters and seawater. A reduction in Nile inflow may either translate the eastward migration of the Canopic branch that supplied the Maryut lagoon (Fig. 1), or a basin-scale reduction in Nile flow, well identified between ~5.5 and ~4.5 ka cal. BP by a lowering of Ethiopian lake levels (Gasse, 2000; Chalié and Gasse, 2002; Marshall et al., 2009, 2011; Fig. 4), wadi desiccation in northern Sudan (Kröpelin and Soulié-Marsche, 1991; Pachur and Hoelzmann, 1991), and a lowering of the main Nile (Said, 1993). Blanchet et al. (2013) used bulk elemental composition, grain-size analyses and strontium and neodymium isotopes from a sediment core collected on the Nile deep-sea fan to reconstruct the progressive decline of Blue Nile discharge between 8 and 4 ka and an arid phase centred on 3.5 ka BP which marks the end of the AHP (Fig. 4). This phase is also recorded in our Sr data, which records the lowest phase of Nile flow between 4 and 3 ka.

On the Nile delta, the water budget of Idku lagoon shifted from marsh to marine-influenced lagoon conditions during this period (Fig. 1; Chen et al., 1992), and the previous river-dominated cuspate delta shifted to a wave-dominated arcuate system (Stanley and Warne, 1993a). These processes occurred when Nile discharge and sediment supply to the coast decreased, leading to more active marine processes. Moreover, decreases in Cyperaceae from a palynological record in the Burullus lagoon (northern delta) have been interpreted as the vegetation response to lower Nile flow during the same period (Bernhardt et al., 2012). In light of the concomitant regional evidence, it is probable that higher seawater inputs into the Maryut were linked to decreasing Nile flow.

The Maryut's $^{87}\text{Sr}/^{86}\text{Sr}$ time series therefore describes the transition from the AHP to regional aridity. Although well identified in far-field sites from the Saharan belt, the rhythm of the AHP's termination remains uncertain. Opinions vary between abrupt climate change (e.g. deMenocal et al., 2000; Garcin et al., 2012) and a non-linear site-specific response to gradual climatic forcing, related to the decline in monsoonal precipitation, which followed the decrease in summer insolation at low latitudes between ca 8 and 4 ka (Stager et al., 2003, Fig. 4; Marriner et al., 2012b; Kröpelin et al., 2008; Marshall et al., 2011; Engel et al., 2012; Hassan et al., 2012; Bernhardt et al., 2012; Blanchet et al., 2013; Revel et al., 2013). In the Maryut, change from a Nile to a marine-dominated lagoon appears to occur gradually between ~5.5 and ~3.8 cal. BP (Fig. 3D). This progressive transition is confirmed by the biomass proxies that gradually increase during the same period (Fig. 3B and C). Our data emphasise the gradual hydrological and ecological responses to the termination of the AHP.

4.3.4. Human impacts since 2 ka

In comparison to the previous period, the upper part of the Maryut stratigraphy has recorded the dominant role of Nile inputs into the lagoon, since at least 2 ka, with $^{87}\text{Sr}/^{86}\text{Sr}$ values being the lowest for the whole sequence. Following the marine-influenced lagoon environment identified up to 2.9 ka cal. BP (Fig. 3), the Sr ratios shift from sea-like values towards the Nile end-member, down to 0.7084, recorded at 1.8–1.7 ka cal. BP. Consistent with this trend, low-brackish fauna characterize the sedimentary unit 4 (Table 1). Towards the top of the unit, $^{87}\text{Sr}/^{86}\text{Sr}$ display values between 0.7081 and 0.7086 that are lower than during the AHP (unit 2). Unfortunately, the sedimentary hiatus does not allow us to

precisely constrain the rhythm of the hydrological changes between units 3 and 4 (Fig. 4). Although Blanchet et al. (2013) demonstrated slightly higher Blue Nile sediment discharge into the Nile deep-sea fan, Nile water flow derived from precipitation proxies does not show significant changes for this period (Fig. 4). We suggest that the construction of the Alexandria canal, attested at least since the early 1st century AD (but possibly dating back to the foundation of Alexandria in the 4th century BC; Hairy and Sennoune, 2006), has been a key factor in the evolution of the Maryut lagoon, because the canal isolated the Maryut from the newly formed Abukir lagoon and therefore from the sea (Fig. 1). At this time, the lagoon was known as Lake Mareotis, used for transportation and whose shores were densely occupied (Empereur, 1998; Khalil, 2008). Lake Mareotis was connected to the Canopic branch through at least two ancient tributaries (Flaux, 2012). The archaeological record attests to harbours and farm complexes close to the lake, with all sites being attributed to Antiquity (Blue and Khalil, 2010; Blue et al., 2011). Given the density of human occupation, we suggest that irrigation practices since early Ptolemaic times (Redon, 2007, pp.450–459), and in particular the digging of a canal between the Canopic branch and Alexandria at least 2 ka ago, probably isolated the Maryut from the sea and led to the desalination of the Maryut lagoon.

A return to dominant marine inputs is recorded between ~1.2 and ~0.7 ka cal. BP (Fig. 4). Gypsum was deposited at the bottom of the Maryut during a retraction of the water body and concentration of marine-derived waters, as suggested by the marine-like Sr isotope composition of the gypsum. This implies both marine incursion into the lagoon and the closure of the Maryut during formation of the evaporite, consistent with a rapidly changing landscape, which follows the Nile-dominated lagoon stage recorded in unit 4. These data therefore reconstruct an important shift in the Maryut's hydrological budget at ~1.2 ka cal. BP. After the Arab conquest (~1.3 ka cal. BP), the export economy of Alexandria's countryside significantly declined. The role of the Maryut lagoon as an important transport interface decreased and fluvial waterways were slowly abandoned (Décobert, 2002). In addition, an agricultural recession has been reported on the northern delta at ~1 ka cal. BP (Toussoun, 1926). In light of this, we suggest that the Maryut sebkha can be linked to the abandonment and siltation of Nile distributaries that reached the Maryut.

Since ~0.7 ka, the Maryut has been reconnected to the Nile (Fig. 4), as demonstrated by Sr isotopic ratios whose values are lower than during the AHP, as well as by the lightly brackish fauna characteristic of sediments from this last period (unit 6; Table 1). This appears coherent with the digging of canals reported by historical sources dating from this time (Guest, 1912; Toussoun, 1926).

Historical accounts for the period between the 15th and the 18th centuries AD attest to significant annual variations in the lagoon surface and Maryut landscape (Flaux et al., 2012). These rapid changes, including the brief seawater flooding of the Maryut basin by the British during the early 1800s (Awad, 2010), could not be resolved by our data.

The last 2 ka have recorded: (1) higher variability in the Sr isotopic composition; and (2) increased freshwater inflow to the Maryut lagoon, compared to the period 7.5–3 ka (Fig. 4). This is probably due to greater anthropogenic controls acting on the hydrology of the Maryut lagoon, in relation to the development of an extensive irrigation network in the western delta after the foundation and growth of Alexandria and its countryside. Furthermore, water diversion from the Canopic branch (Fig. 1) may have accentuated the gradual siltation of the Canopic channel. Blouin (2006) has evoked a similar scenario for the Mendesian branch during Roman times. Reinhardt et al. (1998, 2001) reconstructed the desalinization of the Manzala lagoon, during the second half of the

20th century, resulting from the diversion of Nile water into the irrigation system and downstream to the lagoon (see corresponding $^{87}\text{Sr}/^{86}\text{Sr}$ data shown in Figs. 3 and 4). At a millennial timescale, the increasing diversion of Nile flow by societies since Antiquity probably induced the disappearance of five of the seven branches known in ancient times (Toussoun, 1922).

5. Conclusion

Sr isotope ratios of ostracod shells were analyzed in two cores and one section from the Maryut lagoon, in order to reconstruct palaeohydrological changes. $^{87}\text{Sr}/^{86}\text{Sr}$ ratios are used as proxies for Nile and seawater inputs into the coastal lagoon. In the Maryut's Holocene sequence, the outlier values range from ~0.7080 to ~0.7092, i.e. indicating hydrological changes from a Nile-dominated lagoon to a marine-dominated lagoon. Following the marine transgression of the Maryut and the relative stabilization of sea level between ~7.5 and ~6.8 ka cal. BP, the lagoon's hydrology was mostly controlled by fluctuations in Nile inflow. Our data record high Nile flow up to ~5.5 ka cal. BP, followed by a gradual decrease to ~3.8 ka, probably in relation to the end of the African Humid Period and a transition towards more arid conditions in the Nile watershed. For the last 2 ka, our data support increasing human impacts on Nile flow in the western part of the deltaic plain. The data demonstrate that the Maryut lagoon has recorded a complex hydrological history. Previous palaeoecological interpretations from the same sequence largely corroborate the Sr time series. Although the two methods are complementary, an advantage of the Sr record is its ability to quantify the relative inputs of seawater and freshwater into the system through time. This work shows that strontium isotopes constitute a reliable proxy to reconstruct water-budget changes in the Nile's lagoons, collectively mediated by basin-scale climate change and local to regional-scale human impacts.

Acknowledgements

This study was supported by the French National Research Agency (ANR): project PALEOMED. The ARTEMIS-INSU program financed radiocarbon dates. Pr. Magdy Torab and Mena el-Assal (Alexandria University) are thanked for valuable assistance during fieldwork. The authors would like to thank the CEAlex (CNRS-USR 3134, head J.-Y. Empereur) for logistic help during fieldwork. We also thank Z. Chen, M. Magny, C. Petit, M. Torab and A. Vött, as well as two anonymous reviewers for fruitful comments on earlier versions of the manuscript.

References

- Andersson, P.S., Wasserburg, G.J., Ingri, J., 1992. The sources and transport of Sr and Nd isotopes in the Baltic Sea. *Earth and Planetary Science Letters* 113, 459–472.
- Athersuch, J., Horne, D.J., Whittaker, J.E., 1989. Marine and brackish water ostracods (Superfamilies Cypridacea and Cytheracea). In: Kermack, D.M., Barnes, R.S.K. (Eds.), *Synopses of the British Fauna*, New Series, vol. 43. E. J. Brill, Leiden, pp. 1–343.
- Awad, I., 2010. A study of the evolution of the Maryut Lake through maps. In: Blue, L., Khalil, E. (Eds.), *Lake Mareotis: Reconstructing the Past*, Proceedings of the International Conference on the Archaeology of the Mareotic Region Held at Alexandria University, Egypt 5th–6th April 2008, vol. 2. University of Southampton Series in Archaeology, BAR S2113, Oxford, pp. 11–33.
- Becker, R.H., Sultan, M., 2009. Land subsidence in the Nile delta: inferences from radar interferometry. *The Holocene* 19 (6), 949–954.
- Bernard, A., 1970. Le delta Egyptien d'après les textes grecs. 1-Les confins Lybiques. IFAO, Le Caire, pp. 61–145.
- Bernasconi, M.P., Stanley, J.-D., 1994. Molluscan biofacies and their environmental implications, Nile delta lagoons, Egypt. *Journal of Coastal Research* 10 (2), 440–465.
- Bernhardt, C.E., Horton, B.P., Stanley, J.-D., 2012. Nile delta vegetation response to Holocene climate variability. *Geology* 40 (7), 615–618.
- Blanchet, C.L., Tjallingii, R., Frank, M., Lorenzen, J., Reitz, A., Brown, K., Feseker, T., Brückmann, W., 2013. High- and low-latitude forcing of the Nile River regime during the Holocene inferred from laminated sediments of the Nile deep-sea fan. *Earth and Planetary Science Letters* 364, 98–110.
- Blouin, K., 2006. Homme et milieu dans le nome mendésien à l'époque romaine (1er au 6e S.). PhD thesis. University of Nice Sophia Antipolis, France and University of Laval, Québec, p. 558.
- Blue, L., Khalil, E. (Eds.), 2010. *Lake Mareotis: Reconstructing the Past*. Proceedings of the International Conference on the Archaeology of the Mareotic Region Held at Alexandria University, Egypt, 5th–6th April 2008. Bar international Series 2113, vol. 2. University of Southampton Series in Archaeology, Oxford, p. 156.
- Blue, L., Khalil, E., Trakadas, A. (Eds.), 2011. *A Multidisciplinary Approach to Alexandria's Economic Past: the Lake Mareotis Research Project*. Bar International Series 2285, vol. 5. University of Southampton Series in Archaeology, Oxford, p. 313.
- Box, M.R., Krom, M.D., Cliff, R.A., Bar-Matthews, M., Almogi-Labin, A., Ayalon, A., Paterné, M., 2011. Response of the Nile and its catchment to millennial-scale climatic change since the LGM from Sr isotopes and major elements of East Mediterranean sediments. *Quaternary Science Reviews* 30, 431–442.
- Brass, G.W., 1976. The variation of the marine $^{87}\text{Sr}/^{86}\text{Sr}$ ratio during Phanerozoic time: interpretation using a flux model. *Geochimica et Cosmochimica Acta* 40, 721–730.
- Butzer, K.W., 1976. *Early Hydraulic Civilization in Egypt: a Study in Cultural Ecology*. University of Chicago Press, Chicago, p. 149.
- Butzer, K.W., 2002. Geoarchaeological implications of recent research in the Nile delta. In: Van den Brink, E.C.M., Levy, T.E. (Eds.), *Egypt and the Levant, Interrelations from the 4th through the Early 3rd Millennium BCE*. Leicester University Press, London, pp. 83–97.
- Capo, R.C., DePaolo, D.J., 1990. Seawater strontium isotopic variations from 2.5 million years ago to the present. *Science* 249 (4964), 51–55.
- Capo, R.C., Stewart, B.W., Chadwick, O.A., 1998. Strontium isotopes as tracers of ecosystem processes: theory and methods. *Geoderma* 82, 197–225.
- Chalié, F., Gasse, F., 2002. Late Glacial-Holocene diatom record of water chemistry and lake level change from the tropical East African Rift Lake Abiyata (Ethiopia). *Paleogeography, Palaeoclimatology, Palaeoecology* 187, 259–283.
- Chen, Z., Stanley, J.-D., 1993. Alluvial stiff muds (late Pleistocene) underlying the lower Nile delta plain, Egypt: petrology, stratigraphy and origin. *Journal of Coastal Research* 9 (2), 539–576.
- Chen, Z., Warne, A.G., Stanley, J.-D., 1992. Late quaternary evolution of the northwestern Nile delta between the Rosetta promontory and Alexandria, Egypt. *Journal of Coastal Research* 8 (3), 527–561.
- Conway, D., 2000. The climate and hydrology of the Upper Blue Nile River. *The Geographical Journal* 166, 49–62.
- Décoët, C., 2002. Maréotide médiévale. Des bédouins et des chrétiens. In: Décoët, C. (Ed.), *Etudes Alexandrines 8*, Alexandria Médiévale, vol. 2. IFAO, le Caire, pp. 127–167.
- deMenocal, P., Ortiz, J., Guilderson, T., Adkins, J., Sarnthein, M., Baker, L., Yarusinsky, M., 2000. Abrupt onset and termination of the African Humid Period: rapid climate responses to gradual insolation forcing. *Quaternary Science Reviews* 19, 347–361.
- Durazzi, J.T., 1977. Stable isotope in the ostracode shell, a preliminary study. *Geochimica et Cosmochimica Acta* 41, 1168–1170.
- El-Asmar, H.M., Wood, P., 2000. Quaternary shoreline development: the northwestern coast of Egypt. *Quaternary Science Reviews* 19, 1137–1149.
- Einsele, G., 2000. *Sedimentary Basins. Evolution, Facies and Sediment Budget*. Berlin Heidelberg, Springer-Verlag, p. 792.
- Empereur, J.-Y., 1998. *Alexandrie Redécouverte*. Fayard/Stock, Paris, p. 253.
- Engel, M., Brückner, H., Pint, A., Wellbrock, K., Ginau, A., Voss, P., Grottker, M., Klasen, N., Frenzel, P., 2012. The early Holocene humid period in NW Saudi Arabia – sediments, microfossils and palaeo-hydrological modelling. *Quaternary International* 266, 131–141.
- Faure, G., Powell, J.L., 1972. *Strontium Isotope Geology*. Springer-Verlag, New York, p. 188.
- Flaux, C., Morhange, C., Marriner, N., Rouchy, J.-M., 2011. Bilan hydrologique et bion-sédimentaire de la lagune du Maryut (delta du Nil, Egypte) entre 8000 et 3200 ans cal. B.P. *Géomorphologie: relief, processus et environnement* 3, 261–278.
- Flaux, C., 2012. *Holocene Coastal Palaeo-environment of Maryut Lake in the Northwestern Nile Delta, Egypt*. PhD thesis. Aix-Marseille University, p. 413.
- Flaux, C., El-Assal, M., Marriner, N., Morhange, C., Rouchy, J.-M., Soulié-Märche, I., Torab, M., 2012. Environmental changes in the Maryut lagoon (northwestern Nile delta) during the last ~2000 years. *Journal of Archaeological Science* 39 (12), 3493–3504.
- Fleming, K., Johnston, P., Zwartz, D., Yokoyama, Y., Lambeck, K., Chappell, J., 1998. Refining the eustatic sea-level curve since the Last Glacial Maximum using far – and intermediate – field sites. *Earth and Planetary Science Letters* 163, 327–342.
- Foucault, A., Stanley, J.-D., 1989. Late Quaternary paleoclimatic oscillations in east Africa recorded by heavy minerals in the Nile delta. *Nature* 339, 44–46.
- Frenzel, P., Boomer, I., 2005. The use of ostracods from marginal marine, brackish waters as bioindicators of modern and Quaternary environmental changes. *Paleogeography, Palaeoclimatology, Palaeoecology* 225, 68–92.
- Frihy, O., Deebes, E.A., Shereet, S.M., Abdalla, F.A., 2010. Alexandria-Nile delta coast, Egypt: update and future projection of relative sea-level rise. *Environmental Earth Science* 61, 253–273.
- Frihy, O., Lawrence, D., 2004. Evolution of the modern Nile delta promontories: development of accretional features during shoreline retreat. *Environmental Geology* 46, 914–931.

- Garcin, Y., Melnick, D., Strecker, M.R., Olago, D., Tiercelin, J.J., 2012. East African mid-Holocene wet-dry transition recorded in palaeo-shorelines of Lake Turkana, northern Kenya Rift. *Earth and Planetary Science Letters* 331–332, 322–334.
- Gasse, F., 2000. Hydrological changes in the African tropics since the Last Glacial maximum. *Quaternary Science Reviews* 19, 189–211.
- Gerstenberger, H., Haase, G., El Nour, F.A., 1999. The origin of strontium and the strontium isotope budget of the river Nile. *Isotopes in Environmental and Health Studies* 33, 349–356.
- Goriran, J.-P., 2001. Recherches géomorphologiques dans la région littorale d'Alexandrie en Egypte. PhD thesis. Aix-Marseille University, p. 265.
- Goodfriend, G.A., Stanley, J.-D., 1996. Reworking and discontinuities in Holocene sedimentation in the Nile delta: documentation from amino acid racemization and stables isotopes in mollusks shells. *Marine Geology* 129, 271–283.
- Gosz, J.R., Brookins, D.G., Moore, D.I., 1983. Using strontium isotope ratios to estimate inputs to ecosystems. *Bioscience* 33, 23–30.
- Graustein, W.C., 1989. $^{87}\text{Sr}/^{86}\text{Sr}$ ratios measure the sources and flow of strontium in terrestrial ecosystems. In: Rundel, P.W., Ehleringer, J.R., Nagy, K.A. (Eds.), *Stable Isotopes in Ecological Research*. Springer-Verlag, New York, pp. 491–512.
- Guelorget, O., Perthuisot, J.P., 1983. Le domaine paralique. Expressions géologiques, biologiques et économiques du confinement. *Travaux du laboratoire de Géologie, Ecole Normale Supérieure*, Paris, 16, p. 136.
- Guest, A.R., 1912. The Nile delta during the middle ages: a note on the branches of the Nile and the Kurahs of lower Egypt, with map. *Journal of the Royal Asiatic Society* 44 (04), 941–980.
- Hairy, I., Sennoune, O., 2006. Géographie historique du canal d'Alexandrie. *Annales Islamologiques* 40, 247–278.
- Hart, W.S., Quade, J., Madsen, D.B., Kaufmann, D.S., Ovitt, C.G., 2004. The $^{87}\text{Sr}/^{86}\text{Sr}$ ratios of lacustrine carbonates and lake-level history of the Bonneville paleo-lake system. *Geological Society of America Bulletin* 116, 1107–1119.
- Hassan, F.A., Hamdan, M.A., Flower, R.J., Keatings, K., 2012. Oxygen and carbon isotopic records in Holocene freshwater mollusc shells from the Fayum palaeolakes, Egypt: palaeoenvironmental and palaeoclimatic implications. *Quaternary International* 266, 175–187.
- Herut, B., Starinsky, A., Katz, A., 1993. Strontium in rainwater from Israel: sources, isotopes and chemistry. *Earth and Planetary Science Letters* 120, 77–84.
- Hodell, D.A., Mead, G.A., Mueller, P.A., 1990. Variation in the strontium isotopic composition of seawater (8 Ma to present): implications for geochemical weathering rate and dissolved fluxes to the oceans. *Chemical Geology (Isotope Geoscience Section)* 80, 291–307.
- Holmes, J.A., Darbyshire, D.P.F., Heaton, T.H.E., 2007. Palaeohydrological significance of late quaternary strontium isotope ratios in a tropical lake. *Chemical Geology* 236, 281–290.
- Hori, K., Tanabe, S., Yoshiki, S., Haruyama, S., Nguyen, V., Kitamura, A., 2004. Delta initiation and Holocene sea-level change: example from the Song Hong (Red River) delta, Vietnam. *Sedimentary Geology* 164, 237–249.
- Ingram, B.L., Sloan, D., 1992. Strontium isotopic composition of estuarine sediments as paleosalinity-paleoclimate indicator. *Science* 255, 68–72.
- Khalil, E., 2008. The sea, the River and the Lake: all the waterways lead to Alexandria. On line, 1, vol. Speciale B/B7/5. *Bullettino di Archaeologia*, 33–48.
- Kotb, T.H.S., Watanabe, T., Ogino, Y., Tanji, K.K., 1999. Soil salinization in the Nile delta and related policy issues in Egypt. *Agricultural Water Management* 43, 239–261.
- Krom, M.D., Cliff, R.A., Eijlsink, L.M., Herut, B., Chester, R., 1999. The characterization of Saharan dusts and Nile particulate matter in surface sediments from the Levantine basin using Sr isotopes. *Marine Geology* 155, 319–330.
- Krom, M.D., Stanley, J.-D., Cliff, R.A., Woodward, J.C., 2002. Nile river sediment fluctuations over the past 7000 yr and their key role in sapropel development. *Geology* 30 (1), 71–74.
- Kröpelin, S., Soulié-Marsche, I., 1991. Charophyte remains from wadi Howar as evidence for deep mid-Holocene freshwater lakes in the eastern Sahara of northwest Sudan. *Quaternary Research* 36, 210–223.
- Kröpelin, S., Verschuren, D., Lézine, A.-M., Eggermont, H., Cocquyt, C., Francus, P., Cazet, J.-P., Fagot, M., Rumes, B., Russell, J.M., Darius, F., Conley, D.J., Schuster, M., von Suchodolitz, H., Engstrom, D.R., 2008. Climate-driven ecosystem succession in the Sahara: the past 6000 years. *Science* 320, 765–768.
- Lance, N.C., Banner, J.L., Mack, L.E., 2011. Sr isotopes as tracers of anthropogenic influences on stream water in the Austin, Texas area. *Chemical Geology* 282, 84–97.
- Marriner, N., Flaux, C., Kaniewski, D., Morhange, C., 2012a. The Nile delta's sinking past: quantifiable links with Holocene compaction and climate-driven changes in sediment supply? *Geology* 40, 1083–1086.
- Marriner, N., Flaux, C., Kaniewski, D., Morhange, C., Leduc, G., Moron, V., Chen, Zhongyuan, Gasse, F., Empereur, J.-Y., Stanley, J.-D., 2012b. ITCZ and ENSO-like pacing of Nile delta hydro-geomorphology during the Holocene. *Quaternary Science Reviews* 45, 73–84.
- Marshall, M.H., Lamb, H.F., Davies, S.J., Leng, M.J., Kubisa, Z., Umer, M., Bryant, C., 2009. Climatic change in northern Ethiopia during the past 17,000 years: a diatom and stable isotope record from Lake Ashenge. *Palaeogeography, Palaeoclimatology, Palaeoecology* 279, 114–127.
- Marshall, M.H., Lamb, H.F., Huws, D., Davies, S.J., Bates, R., Bloemendal, J., Boyle, J., Leng, M.J., Umer, M., Bryant, C., 2011. Late Pleistocene and Holocene drought events at Lake Tana, the source of the Blue Nile. *Global and Planetary Change* 78 (3–4), 147–161.
- Morhange, C., Laborel, J., Hesnard, A., 2001. Changes of relative sea level during the past 5000 years in the ancient harbor of Marseilles, Southern France. *Palaeogeography, Palaeoclimatology, Palaeoecology* 166, 319–329.
- Ollivier, P., 2006. Interface continent-océan: Géochimie du rhône (Flux et bilan d'érosion) et transfert d'eaux souterraines en Camargue (apport des isotopes du radium). PhD thesis. Aix-Marseille University, p. 246.
- Pachur, H.J., Hoelzmann, P., 1991. Palaeoclimatic implications of late Quaternary lacustrine sediments in western Nubia, Sudan. *Quaternary Research* 36, 257–276.
- Padoa, M., Garzanti, E., Harlavan, Y., Maria Villa, I., 2011. Tracing Nile sediment sources by Sr and Nd isotope signatures (Uganda, Ethiopia, Sudan). *Geochimica et Cosmochimica Acta* 75, 3627–3644.
- Palmer, M.R., Edmond, J.M., 1989. The strontium isotope budget of the modern ocean. *Earth and Planetary Science Letters* 92, 11–26.
- Redon, B., 2007. Le Delta égyptien aux temps des Grecs. La présence grecque en Basse Égypte, de l'époque saïte à la fin de l'époque hellénistique: diffusion, nature, intensité et conséquences. PhD thesis. University of Lille III, p. 605.
- Reimer, P.J., Baillie, M.G.L., Bard, E., Bayliss, A., Beck, J.W., Blackwell, P.G., Bronk Ramsey, C., Buck, C.E., Burr, G.S., Edwards, R.L., Friedrich, M., Grootes, P.M., Guilderson, T.P., Hajdas, I., Heaton, T.J., Hogg, A.G., Hughen, K.A., Kaiser, K.F., Kromer, B., McCormac, F.G., Manning, S.W., Reimer, R.W., Richards, D.A., Southon, J.R., Talamo, S., Turney, C.S.M., Van der Plicht, J., Weyhenmeyer, C.E., 2009. IntCal09 and Marine09 radiocarbon age calibration curves, 0–50,000 years cal BP. *Radiocarbon* 51 (4), 1111–1150.
- Reinhardt, E.G., Blenkinsop, J., Patterson, R.T., 1999. Assessment of a Sr isotope vital effect in marine taxa from Lee Stocking Island, Bahamas. *Geo-marine Letters* 18, 241–246.
- Reinhardt, E.G., Stanley, J.-D., Patterson, R.T., 1998. Strontium isotopic-paleontological method as a high-resolution paleosalinity tool for lagoonal environments. *Geology* 26 (11), 1003–1006.
- Reinhardt, E.G., Stanley, J.-D., Schwarzc, P., 2001. Human-induced desalinization of Manzala lagoon, Nile delta, Egypt: evidence from isotopic analysis of benthic invertebrates. *Journal of Coastal Research* 17 (2), 431–442.
- Revel, M., Ducassou, E., Grousset, F.E., Bernasconi, S.M., Migeon, S., Revillon, S., Mascle, J., Murat, A., Zaragosi, S., Bosch, D., 2010. 100,000 years of African monsoon variability recorded in sediments of the Nile margin. *Quaternary Science Reviews* 29, 1342–1362.
- Revel, R., Combourieu-Nebout, N., Ducassou, E., Colin, C., Grousset, F.E., Bernasconi, S., Rolland, Y., Migeon, S., Brunet, P., Zhaa, Y., Bosch, D., Mascle, J., 2013. 21,000 years of Ethiopian African monsoon variability recorded in sediments of the western Nile deep sea fan. In: *The Climate of the Mediterranean Region: Recent Progresses and Climate Change Impacts, Special Issue (in press)*.
- Sabatier, P., Dezieule, L., Blanchemanche, P., Siani, G., Condomines, M., Bentaleb, I., Pièques, G., 2010. Holocene variations of radiocarbon reservoir ages in a Mediterranean lagoonal system. *Radiocarbon* 52, 91–102.
- Said, R., 1993. *The River Nile: Geology, Hydrology and Utilization*. Pergamon Press, Oxford, p. 320.
- Shaw, I. (Ed.), 2000. *The Oxford History of Ancient Egypt*. Oxford University Press, Oxford, p. 512.
- Sivan, D., Lambeck, K., Toueg, R., Raban, A., Porath, Y., Shirman, B., 2004. Ancient coastal wells of Caesarea Maritima, Israel, an indicator for relative sea level changes during the last 2000 years. *Earth and Planetary Science Letters* 222, 315–330.
- Sivan, D., Wdowinski, S., Lambeck, K., Galili, E., Raban, A., 2001. Holocene sea-level changes along the Mediterranean coast of Israel, based on archaeological observations and numerical model. *Palaeogeography, Palaeoclimatology, Palaeoecology* 167, 101–117.
- Stager, J.C., Cumming, B.F., Meeker, L.D., 2003. A 10,000-year high-resolution diatom record from Pilkington Bay, Lake Victoria, East Africa. *Quaternary Research* 59, 172–181.
- Stanley, J.-D., Warne, A.G., 1993a. Nile delta: recent geological evolution and human impact. *Science* 260, 630–634.
- Stanley, J.-D., Warne, A.G., 1993b. Sea level and initiation of Predynastic culture in the Nile delta. *Nature* 363, 435–438.
- Stanley, J.-D., Warne, A.G., 1994. Worldwide initiation of Holocene Marine deltas by deceleration of sea-level rise. *Science* 265, 228–231.
- Stanley, J.-D., 1996. Nile delta: extreme case of sediment entrapment on a delta plain and consequent coastal land loss. *Marine Geology* 129, 189–195.
- Stanley, J.-D., Warne, A.G., Schnepf, G., 2004a. Geoarchaeological interpretation of the Canopic, largest of the relict Nile delta distributaries, Egypt. *Journal of Coastal Research* 20 (3), 920–930.
- Stanley, J.-D., Goddio, F., Jorstad, T.F., Schnepf, G., 2004b. Submergence of ancient Greek cities off Egypt's Nile delta – a cautionary tale. *Geological Society of America* 14, 4–10.
- Stanley, J.-D., Toscano, M.A., 2009. Ancient archaeological sites buried and submerged along Egypt's Nile delta coast: gauges of Holocene delta margin subsidence. *Journal of Coastal Research* 25 (1), 158–170.
- Stuiver, M., Reimer, P.J., Reimer, R.W., 2005. CALIB 5.0. WWW program and documentation.
- Svytski, J.P.M., Kettner, A.J., Overeem, I., Hutton, E.W.H., Hannon, M.T., Brakenridge, G.R., Day, J., Vörösmarty, C., Saito, Y., Giosan, L., Nicholls, R.J., 2009. Sinking deltas due to human activities. *Nature Geoscience* 2, 681–686.
- Talbot, M.R., Williams, M.A.J., Adamson, D.A., 2000. Strontium isotope evidence for late Pleistocene re-establishment of an integrated Nile drainage system. *Geology* 28, 343–346.
- Toussoun, O., 1922. Mémoires sur les anciennes branches du Nil, époque ancienne. Mémoire de l'Institut d'Egypte 4, IFAO, Le Caire, p. 212.

- Toussoun, O., 1926. La géographie de l'Egypte à l'époque arabe, tome 1, partie 1. Mémoire de la Société Royale Archéologique d'Alexandrie, tome 8, IFAO, Le Caire, p. 521.
- Trampier, J., 2009. Ancient towns and new methods: a GIS and remote-guided archaeological survey in the western Nile delta. *Journal of the Chicago Colloquium on Digital Humanities and Computer Science* 1 (1), 1–6.
- Warne, A.G., Stanley, J.-D., 1993. Late quaternary evolution of the northwest Nile delta and adjacent coast in the Alexandria region, Egypt. *Journal of Coastal Research* 9, 26–64.
- Weldeab, S., Kay-Christian, E., Hemleben, C., Vennemann, T.W., Schultz, H., 2002. Sr and Nd isotope composition of late Pleistocene sapropels and nonsapropelic sediments from the Eastern Mediterranean sea: implications for detrital influx and climatic conditions in the source areas. *Geochimica et Cosmochimica Acta* 66 (20), 3585–3598.
- Williams, M.A.J., 2009. Late Pleistocene and Holocene environments in the Nile basin. *Global and Planetary Change* 69, 1–15.
- Williams, M.A.J., Williams, F.M., Duller, G.A.T., Munro, R.N., El Tom, O.A.M., Barrows, T.T., Macklin, M., Woodward, J., Talbot, M.R., Haberlah, D., Fluin, J., 2010. Late Quaternary floods and droughts in the Nile valley, Sudan: new evidence from optically stimulated luminescence and AMS radiocarbon dating. *Quaternary Science Reviews* 29, 1116–1137.
- Woodward, J.C., Macklin, M.G., Krom, M.D., Williams, M.A.J., 2007. The Nile: evolution, quaternary river environments and material fluxes. In: Gupta, A. (Ed.), *Large Rivers: Geomorphology and Management*, pp. 261–292.
- Zhao, Y., Colin, C., Liu, Z., Paterne, M., Siani, G., Xie, X., 2012. Reconstructing precipitation changes in northeastern Africa during the Quaternary by clay mineralogical and geochemical investigations of Nile deep-sea fan sediments. *Quaternary Science Reviews* 57, 58–70.
- Zoppi, U., Albani, A., Ammerman, A.-J., Hua, Q., Lawson, E.M., Serandrei Barbero, R., 2001. Preliminary estimate of the reservoir age in the Lagoon of Venice. *Radiocarbon* 43 (2A), 489–494.